Atomic and molecular hydrogen interacting with Pt(111)

R. A. Olsen
Theoretische Chemie, Vrije Universiteit, De Boelelaan 1083, 1081 HV Amsterdam, The Netherlands

G. J. Kroes
Leiden Institute of Chemistry, Gorlaeus Laboratories, Postbus 9502, 2300 RA Leiden, The Netherlands

E. J. Baerends
Theoretische Chemie, Vrije Universiteit, De Boelelaan 1083, 1081 HV Amsterdam, The Netherlands

(Received 13 July 1999; accepted 27 September 1999)

This computational study is motivated by the apparent conflict between an experiment on dissociation of H_2 and D_2 on Pt(111), which suggests a rather corrugated potential energy surface (PES) for the H_2/Pt(111) system, and an experiment showing only weak nonzero-order diffraction of HD scattering from Pt(111). In the calculations we have used density functional theory (DFT) within the generalized gradient approximation (GGA), including scalar relativistic effects and modelling the Pt(111) surface as a slab. We have found that the H_2/Pt(111) PES is both energetically and geometrically corrugated. We have also found that there are reaction paths without or with very low barriers leading to dissociation of H_2 on the Pt(111) surface, but that there are other reaction paths with substantial barriers. By performing extensive calculations on H interacting with a Pt(111) surface we have shown that a DFT/GGA approach that includes scalar relativistic effects is capable of describing the interaction between a hydrogen atom and a Pt(111) surface in a way that is, for the most part, consistent with experiments. © *1999 American Institute of Physics.*
[S0021-9606(99)70648-3]

I. INTRODUCTION

Due to the central role of Pt as a catalyst in hydrogenation reactions, the interaction of hydrogen with Pt surfaces has over the last three decades been investigated in a large number of studies. Of particular interest to our present study are the issues addressed in three papers.

By scattering a beam of molecular HD from Pt(111) Cowin *et al.*[1] found large probabilities for rotationally inelastic scattering. In contrast, they observed only weak nonzero-order diffraction [as mentioned by Cowin *et al.* this is similar to that found previously for $H_2+Ag(111)$;[2] the observed ratio of nonzero-order diffraction to specular scattering was much smaller than for the corrugated $H_2+LiF(001)$ system[3]]. This lead the authors to conclude that the HD/Pt(111) PES is only weakly corrugated. On the other hand, Luntz *et al.*[4] found that the initial sticking coefficient does not scale with the normal component of the incidence energy when dissociating H_2 or D_2 on Pt(111). Momentum parallel to the surface was found to inhibit dissociation. The sensitivity to parallel momentum suggests that the PES is rather corrugated, seemingly in conflict with the results of Cowin *et al.*

In a theoretical study by Darling and Holloway[5] two types of corrugation were investigated; energetic and geometric. On an energetically corrugated PES the barrier height varies across the surface unit cell, but the distance to the surface at which the barrier is located is constant. A geometrically corrugated PES has a barrier height that is constant across the surface unit cell, but the distance to the surface at which the barrier is located is varied. Darling and Holloway showed that momentum parallel to the surface inhibits dissociation in the case that the PES is energetically corrugated. (A later analysis by Gross[6] confirmed their results for normal collision energies ranging from the minimum to the average barrier height in the PES, but showed that parallel momentum actually increases dissociation for higher normal collision energies, and for normal collision energies in the tunneling regime.) In the dynamics calculations the energetically corrugated PES gave rise to stronger diffraction than seen in the experiments of Cowin *et al.* However, Darling and Holloway claimed that the PES could be manipulated to produce a weak corrugation in the low energy regime covered by the diffraction experiment (and thus less diffraction), but a strong corrugation overall. To be able to construct a realistic PES more information from experiments or theoretical calculations was called for.

A main goal of this paper is therefore to investigate the corrugation of the H_2/Pt(111) PES. For this purpose we use DFT within the GGA, including scalar relativistic effects and modelling the Pt(111) surface as a slab. Six-dimensional quantum dynamics calculations employing a DFT/GGA PES have shown that DFT at the GGA level gives a good description of reaction barrier heights for dissociative chemisorption in the H_2/Pd(100),[7] H_2/Cu(100),[8] and H_2/Cu(111)[9] systems. Nevertheless, before we investigate the H_2/Pt(111) PES we check whether DFT can describe the interaction of hydrogen with Pt surfaces accurately, by performing extensive calculations on atomic hydrogen interacting with a Pt(111) surface at the local density approximation (LDA) and GGA levels and at different levels of relativistic approximations. For the same reason we also perform Pt bulk calculations.

The paper is organized as follows. In Sec. II a short presentation of the methods we have employed is given. The

TABLE I. The basis sets used in the Pt bulk calculations. A NAO is a numerical atomic orbital obtained from a Herman–Skillman type calculation (Ref. 15). An STO is a Slater-type orbital with the given exponents (using units of a_0^{-1}). A frozen core approximation has been used for $4f$ and lower lying orbitals.

	$5d$	$6s$	$6p$	$5f$
NAO	yes	yes	no	no
STO	4.95, 1.65	2.65, 1.10	2.50, 1.25	2.00

results of our calculations are given in Sec. III. Our conclusions are given in Sec. IV.

II. COMPUTATIONAL METHOD

The electronic structure calculations presented in this study were performed using BAND.[10–12] In the program the Kohn–Sham equations[13,14] are solved self-consistently for a periodic system. Full three dimensional translational symmetry is used for bulk calculations, whereas a surface is modelled by a slab with translational symmetry in two directions. A flexible basis set of numerical atomic orbitals (NAOs) obtained from numerical Herman–Skillman-type calculations,[15] Slater-type orbitals (STOs), or a combination of both are used in the expansion of the one-electron states. The frozen core approximation can be used for the core electrons of the heavier atoms avoiding the use of pseudopotentials. An accurate Gauss-type numerical integration scheme[12] is used to calculate the matrix elements of the Hamiltonian, and the **k**-space integration can be done accurately using the quadratic tetrahedron method.[16]

The exchange–correlation energy in the LDA is calculated using the Vosko–Wilk–Nusair formulas.[17] In this study we also report results for two GGAs. The first combines the Becke correction[18] for the exchange energy with the Perdew correction[19] for the correlation energy (BP), and the second is the gradient-corrected functional of Perdew *et al.*[20,21] (PW GGA-II, which we will label PW for brevity). The gradient corrections are calculated from the self-consistent LDA density, which has been shown to be an excellent approximation to the binding energies calculated from the self-consistent nonlocal densities.[22] Both scalar relativistic and spin–orbit corrections are calculated using the zeroth-order regular approximation (ZORA).[23–25]

III. RESULTS

A. Pt bulk

The basis set given in Table I, which gives results very close to the basis set limit, was used for the calculation of the lattice constant, the bulk modulus, and the cohesive energy. Since only one Pt atom is needed in the fcc unit cell to perform these calculations a high accuracy with respect to the numerical integration can be obtained easily. With our chosen settings the error is less than 0.03 eV.

The formation energies have been calculated for 12 different lattice constants. The lattice constants are equally spaced and cover a 20% variation around the experimental value. Fitting the 12 values to Murnaghan's equation of state[26] gives us the theoretical lattice constant, the cohesive energy, and the bulk modulus for the three functionals. Three sets of calculations with 12 points each have been performed. One set is for the nonrelativistic limit, the second set includes scalar relativistic corrections, and the third set includes scalar relativistic and spin–orbit effects. The results are given in Table II. The values we obtain for the lattice constant using the LDA and PW functionals including scalar relativistic effects agree well with the values obtained with the same functionals in Refs. 30, 31, and 32. The agreement for the bulk modulus is also satisfactory.

From Table II we see that the nonrelativistic results for the lattice constant and the bulk modulus are in poor agreement with experiments. Strong relativistic bond contraction and bond stiffening have been found for Au and Pt compounds,[33] and our results for Pt bulk confirm this. The difference between the scalar relativistic and scalar relativistic plus spin–orbit results is seen to be almost negligible. The best agreement with the experimental lattice constant and bulk modulus is obtained using the LDA functional at the scalar relativistic or scalar relativistic plus spin–orbit level, but the two GGAs also show reasonable agreement with the experimental values at these levels of relativistic approximations.

The cohesive energy increases by 0.8–1.1 eV when going from the nonrelativistic level to the scalar relativistic level. Including additional spin–orbit effects lowers the cohesive energy by about 0.25 eV. The nonrelativistic BP and PW results are more than 1 eV too low when compared to the experimental value. The nonrelativistic LDA result for

TABLE II. The cohesive energy (E_{coh}), lattice constant (a_{lat}), and bulk modulus (B_0) for Pt from experiments and different levels of theory. The values for the local density approximation (LDA) and two generalized gradient approximations (BP and PW) are given at the non-relativistic level (nr), the level including scalar relativistic corrections (sr), and the level including scalar relativistic and spin–orbit effects (so). The atomic reference energies are obtained according to Ref. 27 for the nr and sr results, and according to Ref. 28 for the so results.

	E_{coh} [eV/atom]			a_{lat} [a_0]			B_0 [Mbar]		
	5.85			7.41			2.78		
Experiment[a]	nr	sr	so	nr	sr	so	nr	sr	so
LDA	5.98	7.10	6.85	7.69	7.36	7.37	1.81	2.98	3.09
BP	4.49	5.33	5.06	7.93	7.53	7.54	1.28	2.32	2.30
PW	4.67	5.57	5.30	7.91	7.52	7.52	1.31	2.37	2.36

[a]From Ref. 29.

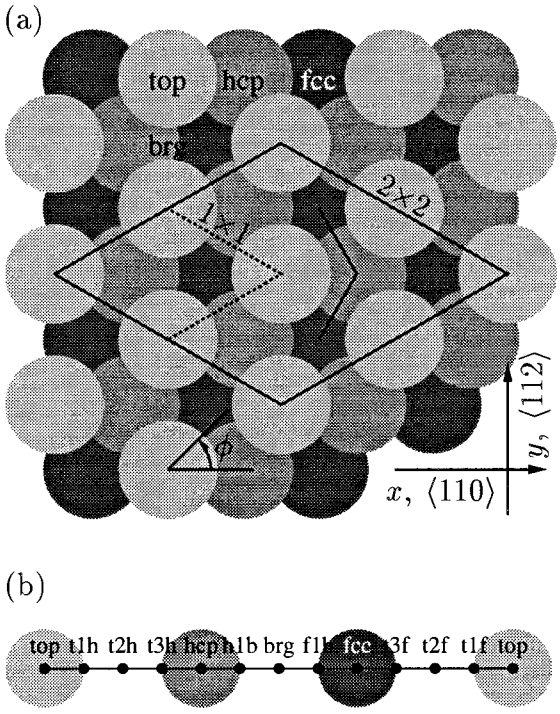

FIG. 1. (a) Top view of the Pt(111) surface, indicating the top, the bridge (brg), the fcc threefold hollow, and the hcp threefold hollow site together with the two different surface unit cells used in the slab calculations. Also shown is the azimuthal angle ϕ, which is the angle the hydrogen molecular bond axis form with the $\langle 110 \rangle$ direction, and a possible diffusion path going from one fcc site to another via two bridge sites and one hcp site. (b) The 12 adsorption sites used in the calculations on the 2×2 and 1×1 surface unit cells are shown.

the cohesive energy is the one that comes the closest to the experimental value, but this must be considered fortuitous, the well-known LDA overbinding compensating for the underbinding at the nonrelativistic level. For the calculations including scalar relativistic or scalar relativistic plus spin–orbit effects it is seen that the LDA overestimates the cohesive energy, whereas the two GGAs gives values that are too low compared to the experimental value. The underestimation of the cohesive energy at the GGA level has also been reported for other sixth row elements.[34]

B. H on Pt(111)

We have determined the adsorption energy, the adsorption height above the surface, and the vibrational frequency normal to the surface for H adsorbing at different surface sites. For this purpose we have employed a three layer slab with a 2×2 surface unit cell as illustrated in Fig. 1(a). To investigate the effect the coverage has on these properties we have also performed calculations using a 1×1 surface unit cell. By performing test calculations for four different adsorption sites the numerical accuracy of the real space integration has been verified to be within 0.01 eV. For the 2×2 surface unit cell 15 points in the irreducible wedge of the surface Brillouin zone has been used for the **k**-space integration giving an accuracy of about 0.02 eV when comparing to more accurate calculations. With 28 points in the irreducible wedge of the surface Brillouin zone the **k**-space integration for the 1×1 surface unit cell is accurate to about 0.03 eV. The basis set labeled 2 in Table III has been used to calculate the adsorption energy, the adsorption height, and the vibrational frequency. The basis set labeled 1 has been used to test the convergence with respect to the basis set. The adsorption energy changes by less than 0.02 eV when going from basis set 1 to 2 for four different adsorption sites. All in all the adsorption energies should be converged to within 0.05 eV of the LDA and GGA limits for H adsorbing on a three layer Pt(111) slab. Changing the number of layers from three to five changes the adsorption energy by less than 0.05 eV, a result that is similar to what has been reported for the H/Pd(111) system.[35] The experimental Pt bulk lattice constant, $a_{\mathrm{lat}}=7.41\ a_0$,[29] has been used for the slab.

The adsorption energies, equilibrium heights, and vibrational frequencies normal to the surface have been calculated for the 12 adsorption sites given in Fig. 1(b) using the 2×2 surface unit cell corresponding to a coverage $\Theta=0.25$. The zero of the energy scale is set to the bottom of the H_2 gas phase potential, i.e., $E_{\mathrm{ad}}(\mathrm{H\ on\ Pt})=-[D_{\mathrm{e}}(\mathrm{H–Pt})-D_{\mathrm{e}}(\mathrm{H_2})/2]$. Thus, negative adsorption energies correspond to the adsorbed hydrogen atom being energetically stable with respect to the free hydrogen molecule. No zero point energy effects have been included in the adsorption energy. Figure 2 shows the results including scalar relativistic effects. The results for the top, fcc, hcp, and bridge sites are also given in

TABLE III. The basis sets used in the slab calculations. A NAO is a numerical atomic orbital obtained from a Herman–Skillman-type calculation (Ref. 15). An STO is a Slater-type orbital with the given exponents (using units of a_0^{-1}). For the Pt basis set labeled 1 a frozen core approximation has been used for $4d$ and lower lying orbitals. The Pt basis set labeled 2 has a $4f$ frozen core.

	Pt	$5s$	$5p$	$4f$	$5d$	$6s$	$6p$	$5f$
1	NAO	yes	yes	yes	yes	yes	no	no
	STO	no	no	no	4.95, 1.65	2.65, 1.10	2.50, 1.25	2.00
2	NAO	no	no	no	yes	yes	no	no
	STO	no	no	no	1.8	2.1	2.1	no
	H	$1s$	$2p$	$3d$				
1	NAO	yes	no	no				
	STO	1.58, 0.69	1.25	2.5				
2	NAO	yes	no	no				
	STO	1.58	1.0	no				

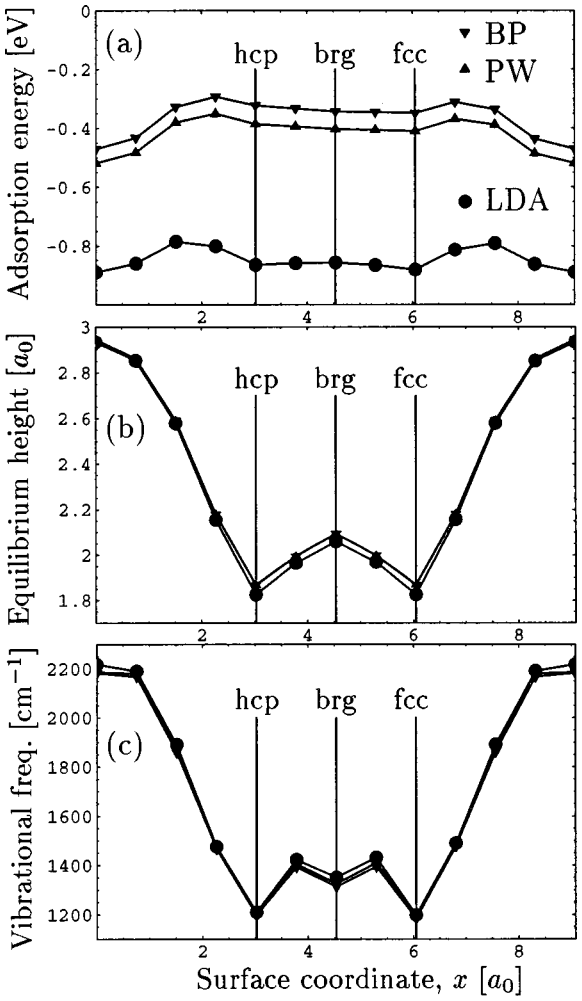

FIG. 2. The adsorption energy per H atom (a), equilibrium height above the surface (b), and vibrational frequency normal to the surface (c) are shown for the 12 adsorption sites given in Fig. 1(b). The top site corresponds to $x=0a_0$ and $x=9.075a_0$. The zero of the energy scale is set to the bottom of the H_2 gas phase potential, and no zero point energy effects have been included. The results include scalar relativistic effects.

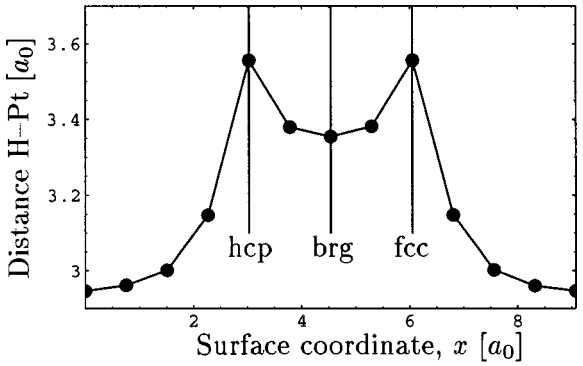

FIG. 3. The equilibrium distance to the nearest Pt atom as computed at the BP level is shown for the 12 adsorption sites given in Fig. 1(b). The top site corresponds to $x=0a_0$ and $x=9.075a_0$. The results include scalar relativistic effects.

Table IV. We find that the magnitude of the adsorption energy is the largest for the top site for all three functionals, with the fcc site being a local minimum which is 0.01 eV, 0.12 eV, and 0.11 eV less stable for the LDA, BP, and PW functionals, respectively. For the LDA the zero point energy associated with motion normal to the surface is 0.06 eV higher at the top site than at the fcc site, thus the LDA predicts the fcc site to be the most stable adsorption site. The difference in the zero point energies between the top and fcc sites is also 0.06 eV at the BP and PW levels, but this is not enough to stabilize the fcc site compared to the top site. However, it is important to note that the differences in the adsorption energies are very small, in the order of the numerical precision of our calculations. It is therefore difficult to reach a conclusion on the preferred adsorption site based on the energetics alone. But a conclusion that *can* be drawn is that the variation in the adsorption energy across the surface unit cell is small. Next we compare the absolute value of the adsorption energy to experiments. Apart from the value of -0.23 ± 0.01 eV reported in Ref. 36, the experimental results for the adsorption energy lie between -0.30 and -0.43 eV at low coverages.[37–42] Thus we see that the LDA clearly overestimates the interaction energy, whereas the BP and PW results are in much better agreement with the experimental values.

The experimental results for the adsorption height above the surface are $2.19\pm0.06a_0$,[41] $1.34a_0$,[43] $1.32\pm0.38a_0$,[44] and $1.10\pm0.08a_0$.[45] In Fig. 2(b) and Table IV it is shown that BP and PW predict almost identical adsorption heights while LDA gives marginally lower values. The adsorption height for the top site clearly falls outside the range of experimental values. In Fig. 3 the equilibrium distance to the

TABLE IV. The adsorption energy (E_{ad}), equilibrium height above the surface (z_{eq}), and vibrational frequency normal to the surface ($\tilde{\nu}_\perp$) are given for four adsorption sites, and for the local density approximation (LDA) and two generalized gradient approximations (BP and PW). The results include scalar relativistic effects. The 2×2 surface unit cell corresponding to a coverage $\Theta=0.25$ has been used in the calculations. The zero of the energy scale is set to the bottom of the H_2 gas phase potential, and no zero point energy effects have been included.

	E_{ad} [eV/H atom]			z_{eq} [a_0]			$\tilde{\nu}_\perp$ [cm^{-1}]		
Site	LDA	BP	PW	LDA	BP	PW	LDA	BP	PW
top	−0.89	−0.47	−0.52	2.93	2.95	2.94	2218	2183	2185
fcc	−0.88	−0.35	−0.41	1.83	1.87	1.87	1199	1184	1192
hcp	−0.86	−0.32	−0.39	1.83	1.87	1.87	1210	1198	1197
brg	−0.86	−0.34	−0.40	2.06	2.09	2.09	1351	1313	1325

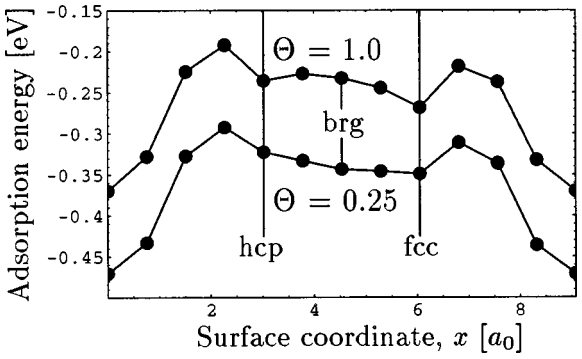

FIG. 4. The adsorption energy computed at the BP level is shown for the 12 adsorption sites given in Fig. 1(b) for monolayer coverage, $\Theta=1.0$, and for $\Theta=0.25$. The zero of the energy scale is set to the bottom of the H_2 gas phase potential, and no zero point energy effects have been included.

nearest Pt atom is given at the BP level. The experimental H–Pt bond distance is $3.2–3.6a_0$ (Refs. 41,43–45) and we see that only the hcp, h1b, brg, f1b, and fcc sites have an H–Pt bond distance falling within this range.

Studies employing electron energy-loss spectroscopy[43,46] and infrared reflection adsorption spectroscopy[47] all report a hydrogen vibrational band in the range 1230–1254 cm^{-1}, even though they do not agree on the vibrational mode to which this vibrational band should be assigned. Our calculated vibrational frequencies normal to the surface are shown in Fig. 2(c) and Table IV. The vibrational frequencies at the threefold hollow sites come close to these experimental values; the frequency calculated for the top site falls far outside the range of experimental values.

The experimentalists have found that the magnitude of the adsorption energy decreases with increasing coverage.[36,38–40] In Fig. 4 and from comparison of the scalar relativistic results in Tables IV and V we see that our calculations show the same trend. For all adsorption sites considered here the adsorption energy at a monolayer coverage, $\Theta=1.0$, is about 0.1 eV per H atom less stable than the adsorption energy at a coverage of $\Theta=0.25$.

From Fig. 2(a) (and the results for $\Theta=0.25$ given at the BP level in Fig. 4) we see that a hydrogen atom moving from one top site to another encounters a barrier of about 0.17 eV at the BP and PW levels, at the LDA level the barrier is about 0.10 eV. A hydrogen atom moving from one fcc site to another via two bridge sites and one hcp site [see Fig. 1(a)] sees a very small barrier of about 0.03 eV at all the three levels of DFT approximations. An experimental value for the barrier to diffusion along the surface of 0.15 eV per H atom was given in Ref. 48. In a more recent study the barrier for diffusion from one fcc site to another was measured to be 68 ± 5 meV,[49] bringing experiment and theory closer together. Finally, additional calculations show that hydrogen placed in the octahedral subsurface site is unstable by 0.86 eV per H atom compared to the bottom of the H_2 gas phase potential (at the BP level, $\Theta=0.25$, and no relaxations included). Thus we find no support for the suggestion of early results[50] that H would penetrate subsurface. Our finding is in agreement with the results of many later studies.[38,45,51–54]

We have also investigated the importance of relativistic effects for the H/Pt(111) system. In Table V results are given for the top and fcc sites, for (i) the nonrelativistic level, (ii) the level including scalar relativistic effects, and (iii) the level including scalar relativistic and spin–orbit effects, at a coverage of $\Theta=1.0$. We see that at the nonrelativistic level the fcc site is clearly preferred above the top site, but the LDA, BP, and PW adsorption energies all lie outside the experimental range of -0.3 to -0.43 eV (taking into account that the adsorption energy is about 0.1 eV smaller in magnitude at monolayer coverage than at a coverage of $\Theta=0.25$). Results of calculations including scalar relativistic or scalar relativistic plus spin–orbit effects and performed at the GGA level show the top site to be preferred over the fcc site, in contrast to the nonrelativistic results. This result is similar to the change of site preference observed in calculations on CO adsorbing on Pt(111).[25] At the nonrelativistic level CO adsorbed in the hollow site, but when including scalar relativistic or scalar relativistic plus spin–orbit effects the top site was the preferred adsorption site. Note however that the fcc site is the most stable site when scalar relativistic and spin–orbit effects are included if the calculation on H/Pt(111) is performed at the LDA level. Comparing to experiment we see that the LDA results including scalar relativistic and spin–orbit effects still overestimate the interac-

TABLE V. The adsorption energy (E_{ad}), equilibrium height above the surface (z_{eq}), and vibrational frequency normal to the surface ($\tilde{\nu}_\perp$) are given for the top and fcc sites, and for the local density approximation (LDA) and two generalized gradient approximations (BP and PW). The results are given at the nonrelativistic level (nr), the level including scalar relativistic effects (sr), and the level including scalar relativistic and spin–orbit effects (so). The 1×1 surface unit cell, which corresponds to a coverage $\Theta=1.0$, has been used in the calculations. The zero of the energy scale is set to the bottom of the H_2 gas phase potential, and no zero point energy effects have been included.

		E_{ad} [eV/H atom]			z_{eq} [a_0]			$\tilde{\nu}_\perp$ [cm^{-1}]		
Site	Level	LDA	BP	PW	LDA	BP	PW	LDA	BP	PW
top	nr	−0.20	0.24	0.19	3.03	3.05	3.05	2025	1965	1963
	sr	−0.80	−0.37	−0.42	2.92	2.94	2.94	2304	2259	2259
	so	−0.71	−0.29	−0.34	2.94	2.95	2.95	2263	2234	2234
fcc	nr	−0.58	−0.03	−0.09	1.87	1.91	1.91	1163	1157	1162
	sr	−0.81	−0.27	−0.33	1.81	1.84	1.84	1186	1184	1189
	so	−0.75	−0.21	−0.27	1.80	1.84	1.84	1199	1194	1197

tion energy, but the BP and PW results lie within the range of the experimental values (also when taking into account that the adsorption energy is about 0.1 eV smaller in magnitude at monolayer coverage than at a coverage of $\Theta=0.25$). Table V shows that the equilibrium height above the surface and the vibrational frequency normal to the surface are left almost unchanged when going from the scalar relativistic to the scalar relativistic plus spin–orbit level. The magnitude of the adsorption energies decrease by less than 0.1 eV.

Summarizing the results in this section we see that, at the LDA as well as the GGA level, our DFT results for the adsorption height above the surface and the vibrational frequency normal to the surface are consistent with H occupying the fcc or the hcp site, in agreement with experiments.[41,43,44,51] The DFT results agree well with the measured adsorption height, H–Pt bond distance and vibrational frequency normal to the surface. As mentioned above, different experimental and theoretical studies do not agree on the vibrational mode to which the frequencies in the range 1230–1254 cm^{-1} should be assigned. The DFT results presented here suggest that these vibrational frequencies arise from a hydrogen atom vibrating normal to the surface, at odds with the conclusions in Refs. 43 and 46, but in agreement with Refs. 47 and 55. The decrease in the magnitude of the adsorption energy with increasing coverage seen in experiments[36,38–40] is also seen in our DFT calculations. And finally, assuming that the barrier to diffusion that is measured pertains to a diffusion path going from one fcc site to another via two bridge sites and one hcp site [see Fig. 1(a)], our calculated diffusion barrier compares favorably to the experimental results of Ref. 49.

The LDA overestimates the interaction energies at all levels of relativistic approximations, but does agree with experiments on the fcc site being the preferred adsorption site. The nonrelativistic results for the two GGAs give too small adsorption energies and the scalar relativistic results somewhat too large adsorption energies. The calculated GGA adsorption energies including scalar relativistic and spin–orbit effects fall within the range of experimental values. For energetics alone the scalar relativistic and scalar relativistic plus spin-orbit levels indicate a preference for the top site, albeit small. However, we should keep in mind that the energy differences we are discussing are less than 0.1 eV and that we probably should not expect DFT to give perfect agreement with experiments at this level of accuracy. When evaluating the predictive force of DFT for a particular system, one should look at a range of properties of that system, and not just focus on the energetics.

All in all this suggests that DFT at the BP or PW level including scalar relativistic or scalar relativistic plus spin–orbit effects is capable of providing a description of the H/Pt(111) system that is, for the most part, consistent with the experimental results for this system. At the scalar relativistic plus spin–orbit level the calculations become far too expensive when we consider systems larger than Pt bulk or hydrogen adsorbed on a Pt(111) slab with $\Theta=1.0$, and this level of theory offers no significant improvement over the scalar relativistic level. Thus, the level of theory we will use in the following section to describe the PES for the H_2/Pt(111) system is DFT at the BP or PW level including scalar relativistic effects.

C. H_2 on Pt(111)

The calculations reported in this section have been carried out using a three layer slab with a 2×2 surface unit cell as described in Sec. III B. The same integration parameters and basis set have also been employed and additional convergence tests show the interaction energies to be accurate to within 0.05 eV of the GGA limits for the H_2/Pt(111) system. As in the preceding section the experimental Pt bulk lattice constant, $a_{lat}=7.41a_0$,[29] has been used for the slab.

To investigate the corrugation of the H_2/Pt(111) PES we have calculated 5 two-dimensional (2D) PESs. The two geometric parameters that are varied are Z and r, the height of the hydrogen molecule's center of mass above the surface and the hydrogen molecule's bond distance, respectively. Each 2D PES is based on between 50 and 60 calculated points and fitted using bicubic splines. For each 2D PES the center of mass of the hydrogen molecule is kept fixed above the top, t2h, brg, fcc, and t2f sites, respectively (see Fig. 1). The reason for leaving out the hcp site is given below. The molecular bond axis forms an angle with the surface normal of $\theta=90$ degrees and lies along the $\langle 112\rangle$ direction [$\phi=90$ degrees, see Fig. 1(a)]. The azimuthal anisotropy of the H_2/Pt(111) PES has been investigated by calculating two additional 2D PESs above the top and bridge sites with $\theta=90$ degrees and the axis along the $\langle 110\rangle$ direction [$\phi=0$ degrees, see Fig. 1(a)]. In Fig. 5 contour plots of six of the seven computed PESs are shown, and the position of the barrier and its height are given in Table VI.

From Table VI and Fig. 5 we see that the top site has the lowest barrier to dissociation. At the BP level it is about 0.06 eV, independent of whether the molecule dissociates towards two bridge sites [$\phi=90$ degrees; see Fig. 5(a)] or towards a fcc and a hcp site [$\phi=0$ degrees; see Fig. 5(b)], suggesting that there is no or very little azimuthal anisotropy above the top site. At the PW level we find no barrier, in agreement with Refs. 56 and 57. The calculations show a small well in the entrance channel for the PW functional, about 0.04 eV below the bottom of the H_2 gas phase potential, but since this is in the range of the accuracy of our calculations we should be careful not to put too much trust in this result. For hydrogen molecules dissociating towards fcc sites above the t2h site and hydrogen molecules dissociating towards hcp sites above the t2f site, the 2D PESs are very similar (we therefore only show the t2f PES in Fig. 5), the barriers being 0.19 and 0.20 eV at the BP level, respectively. Since the dissociation above these two similar (t2f and t2h) sites to the hcp and fcc sites occurs with almost the same barrier height, and because the adsorption energy, adsorption height above the surface, and vibrational frequency normal to the surface are all very similar for H adsorbing at the fcc and hcp sites, we can reasonably assume that the dissociation above the hcp and fcc sites will be very similar. For this reason, calculations were only performed for dissociation above the fcc site [Fig. 5(e)], for which we obtain the highest barrier height (0.42 eV at the BP level). Dissociation towards a hcp and a fcc site

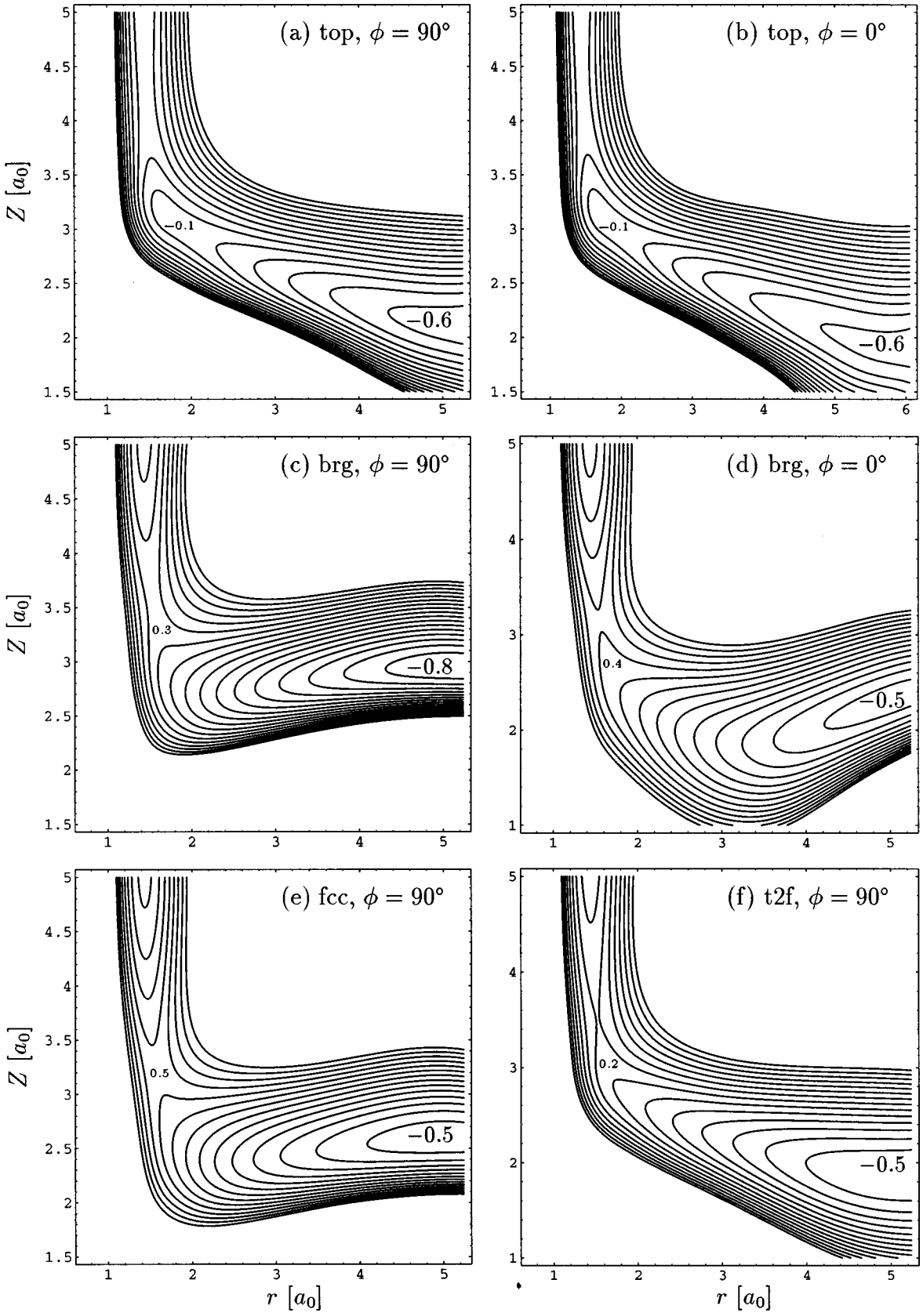

FIG. 5. Contour plots of the 2D PESs computed at the BP level are shown. The height of the hydrogen molecule's center of mass above the surface is denoted by Z, the hydrogen molecule's bond distance by r, and the angle the hydrogen bond axis forms with the $\langle 110 \rangle$ direction by ϕ. All results are for $\theta = 90$ degrees. The first contour line in the entrance channel is 0.1 eV and the contour spacing is 0.1 eV. The numbers within the contour plots are in eV and give the value of the contour line (lines) that lies (lie) closest by. The energies are relative to the bottom of the H_2 gas phase potential. The sites are shown in Fig. 1.

TABLE VI. The position (Z and r) and height (E_b) of the barrier to hydrogen dissociation are given at the BP and PW level. The sites are shown in Fig. 1. All results are for $\theta=90$ degrees. The angle the hydrogen bond axis forms with the $\langle 110\rangle$ direction is denoted by ϕ, the height of the hydrogen molecule's center of mass above the surface by Z, and the hydrogen molecule's bond distance by r. The energies are relative to the bottom of the H_2 gas phase potential.

		BP			PW		
Site	ϕ [degrees]	Z [a_0]	r [a_0]	E_b [eV]	Z [a_0]	r [a_0]	E_b [eV]
top	90	4.25	1.46	0.06	4.33	1.46	−0.02
t2h	90	3.52	1.52	0.19	3.58	1.51	0.11
brg	90	3.53	1.55	0.27	3.57	1.54	0.19
fcc	90	3.21	1.58	0.42	3.25	1.57	0.33
t2f	90	3.51	1.55	0.20	3.57	1.51	0.11
top	0	4.31	1.46	0.06	4.38	1.46	−0.02
brg	0	3.14	1.55	0.40	3.18	1.55	0.31

above a bridge site [Fig. 5(d)] also shows a large barrier, about 0.40 eV, while dissociation towards two top sites above a bridge site [Fig. 5(c)] is hindered by a barrier of about 0.27 eV (both numbers given at the BP level). This indicates a weak azimuthal anisotropy above the bridge site. From Table VI we see that the PW functional gives about 0.1 eV lower barriers for all 2D PESs considered here.

From Table VI and Fig. 5 we see that our calculations agree with experiments that there exist reaction paths without or with very low barriers leading to dissociation of H_2 on the Pt(111) surface.[4,36,37,58,59] Also in agreement with experiments, we find that there are also reaction paths with substantial barriers to dissociation, i.e., the dissociation takes place over a distribution of barriers varying in magnitude.[4,42] In Ref. 4 the sticking coefficient was found to be independent of the initial vibrational state of the incident molecule, indicating that the barriers are located in the entrance channel, and from Fig. 5 we see that our results agree with this conclusion.

The suggestion of Darling and Holloway[5] that the H_2/Pt(111) PES is mainly energetically corrugated is not supported by our results in Table VI and Fig. 5. In their calculations Darling and Holloway use the term geometrically corrugated for a PES where the distance to the surface at which the barrier is located varies with $0.5a_0$ across the surface unit cell. In our calculations at the BP level the distance to the surface at which the barrier is located varies from $3.21a_0$ (above the fcc site) to $4.25a_0$ (above the top site) for $\phi=90$ degrees. Thus, we find the H_2/Pt(111) PES also to be geometrically corrugated. Whether a PES with this combination of energetic and geometric corrugation will give rise to only weak nonzero-order diffraction of HD as seen in Ref. 1 will be investigated by dynamics calculations.[60]

IV. CONCLUSIONS

A main goal of this paper has been to investigate the corrugation of the H_2/Pt(111) potential energy surface (PES). We have used density functional theory (DFT) within the generalized gradient approximation (GGA), including scalar relativistic effects, and modelling the Pt(111) surface as a slab. We found that the H_2/Pt(111) PES is both energetically and geometrically corrugated. Thus, our results do not support the suggestions based on the theoretical calculations by Darling and Holloway[5] that the H_2/Pt(111) is mainly energetically corrugated. But our results are in agreement with the experimental results of Luntz *et al.*[4] on dissociation of H_2 or D_2 on Pt(111) that suggest a rather corrugated PES. The experimental results of Cowin *et al.*[1] seeing only weak nonzero-order diffraction of HD scattering from Pt(111) remain unexplained, but this issue will be addressed in the future[60] with the help of quantum mechanical wave packet calculations employing a DFT/GGA PES which is based on the results presented here.

In agreement with experiments on H_2 + Pt(111), we found that there are reaction paths without or with very low barriers as well as reaction paths with substantial barriers to dissociation, i.e., the dissociation takes place over a distribution of barriers varying in magnitude. Also in agreement with experiments, we found that the barriers are located in the entrance channel. Furthermore, our results show the H_2/Pt(111) PES to have no or very little azimuthal anisotropy above the top site. Above the bridge site the PES shows a weak azimuthal anisotropy. We also find that the Becke–Perdew[18,19] (BP) GGA gives barriers to dissociation which are about 0.1 eV higher than the Perdew–Wang[20,21] (PW) GGA for this system.

To investigate whether DFT can accurately describe the interaction of hydrogen with Pt surfaces we have performed extensive calculations on H interacting with a Pt(111) surface at the local density approximation (LDA), BP and PW levels. All three levels of theory agree well with the measured adsorption height, H–Pt bond distance and vibrational frequency normal to the surface, and these results suggest that the fcc or hcp site is the site H occupies, in agreement with experiments. When considering the energetics we saw that the LDA overestimates the adsorption energies, but gives the right preference for adsorption site—the threefold hollow sites. The two GGAs give reasonable agreement for the adsorption energies, but suggest the top site to be slightly preferred compared to the threefold hollow sites. However, the differences in the adsorption energies are very small, and it is therefore difficult to reach a conclusion on the preferred adsorption site based on the energetics alone. As expected we found scalar relativistic effects to be important, whereas including additional spin–orbit interaction changed the adsorption energies by less than 0.1 eV. All in all these results

suggest that DFT at the BP or PW level including scalar relativistic effects is capable of describing the interaction between a hydrogen atom and a Pt(111) surface in a way that is, for the most part, consistent with experiments.

ACKNOWLEDGMENTS

We gratefully acknowledge the help of Pieter Vernooijs and Erik van Lenthe in obtaining the atomic reference energies used in Table II. We would also like to thank the authors of Ref. 49 for providing us with their paper prior to publication. The calculations reported here have been carried out under a grant of computer time by the Dutch National Computing Facilities Foundation (NCF). The research of R.A.O. is financed by the National Research School Combination ''Catalysis Controlled by Chemical Design'' (NRSC-Catalysis).

[1] J. P. Cowin, C. F. Yu, S. J. Sibener, and L. Wharton, J. Chem. Phys. **79**, 3537 (1983).
[2] J. M. Horne, S. C. Yerkes, and D. R. Miller, Surf. Sci. **93**, 47 (1980).
[3] G. Boato, P. Cantini, and L. Mattera, J. Chem. Phys. **65**, 544 (1976).
[4] A. C. Luntz, J. K. Brown, and M. D. Williams, J. Chem. Phys. **93**, 5240 (1990).
[5] G. R. Darling and S. Holloway, Surf. Sci. Lett. **304**, L461 (1994).
[6] A. Gross, J. Chem. Phys. **102**, 5045 (1995).
[7] A. Gross,. S. Wilke, and M. Scheffler, Phys. Rev. Lett. **75**, 2718 (1995).
[8] G. J. Kroes, E. J. Baerends, and R. C. Mowrey, Phys. Rev. Lett. **78**, 3583 (1997); **81**, 4781(E) (1998).
[9] J. Dai and J. C. Light, J. Chem. Phys. **107**, 1676 (1997).
[10] G. te Velde, Ph.D. thesis, Vrije Universiteit, Amsterdam, 1990.
[11] G. te Velde and E. J. Baerends, Phys. Rev. B **44**, 7888 (1991).
[12] G. te Velde and E. J. Baerends, J. Comput. Phys. **99**, 84 (1992).
[13] P. Hohenberg and W. Kohn, Phys. Rev. **136**, B864 (1964).
[14] W. Kohn and L. J. Sham, Phys. Rev. A **140**, A1133 (1965).
[15] F. Herman and S. Skillman, *Atomic Structure Calculations* (Prentice Hall, New Jersey, 1963).
[16] G. Wiesenekker, G. te Velde, and E. J. Baerends, J. Phys. C **21**, 4263 (1988).
[17] S. H. Vosko, L. Wilk, and M. Nusair, Can. J. Phys. **58**, 1200 (1980).
[18] A. D. Becke, Phys. Rev. A **38**, 3098 (1988).
[19] J. P. Perdew, Phys. Rev. B **33**, 8822 (1986).
[20] J. P. Perdew, in *Electronic Structure of Solids '91*, edited by P. Ziesche and H. Eschrig (Akademie Verlag, Berlin, 1991).
[21] J. P. Perdew *et al.*, Phys. Rev. B **46**, 6671 (1992).
[22] B. Hammer, M. Scheffler, K. W. Jacobsen, and J. K. Nørskov, Phys. Rev. Lett. **73**, 1400 (1994).
[23] E. van Lenthe, Ph.D. thesis, Vrije Universiteit, Amsterdam, 1996.
[24] E. van Lenthe, E. J. Baerends, and J. G. Snijders, J. Chem. Phys. **101**, 9783 (1994).
[25] P. H. T. Philipsen, E. van Lenthe, J. G. Snijders, and E. A. Baerends, Phys. Rev. B **56**, 13556 (1997).
[26] F. D. Murnaghan, Proc. Natl. Acad. Sci. USA **3**, 244 (1944).
[27] E. J. Baerends, V. Branchadell, and M. Sodupe, Chem. Phys. Lett. **265**, 481 (1997).
[28] E. van Lenthe, J. G. Snijders, and E. J. Baerends, J. Chem. Phys. **105**, 6505 (1996).
[29] C. Kittel, *Introduction to Solid State Physics*, 6th ed. (Wiley, New York, 1986).
[30] V. Ozoliņš and M. Körling, Phys. Rev. B **48**, 18304 (19983).
[31] A. Khein, D. J. Singh, and C. J. Umrigar, Phys. Rev. B **51**, 4105 (1995).
[32] G. Boisvert, L. J. Lewis, and M. Scheffler, Phys. Rev. B **57**, 1881 (1998).
[33] P. Pyykkö, Chem. Rev. **88**, 563 (1988).
[34] P. H. T. Philipsen and E. J. Baerends, Phys. Rev. B (in press).
[35] J. F. Paul and P. Sautet, Phys. Rev. B **53**, 8015 (1996).
[36] K. Christmann, G. Ertl, and T. Pignet, Surf. Sci. **54**, 365 (1976).
[37] R. W. McCabe and L. D. Schmidt, Surf. Sci. **65**, 189 (1977).
[38] P. R. Norton, J. A. Davies, and T. E. Jackman, Surf. Sci. **121**, 103 (1982).
[39] B. J. J. Koeleman *et al.*, Nucl. Instrum. Methods Phys. Res. **218**, 225 (1983).
[40] S. C. Gebhard and B. E. Koel, J. Phys. Chem. **96**, 7056 (1992).
[41] K. Umezawa *et al.*, Surf. Sci. **387**, 320 (1997).
[42] P. Samson, A. Nesbitt, B. E. Koel, and A. Hodgson, J. Chem. Phys. **109**, 3255 (1998).
[43] A. M. Baró, H. Ibach, H. D. Bruchmann, Surf. Sci. **88**, 384 (1979).
[44] B. J. J. Koeleman *et al.*, Phys. Rev. Lett. **56**, 1152 (1986).
[45] K. Mortensen, F. Besenbacher, I. Stensgaard, and C. Klink, Surf. Sci. **211/212**, 813 (1989).
[46] L. J. Richter and W. Ho, Phys. Rev. B **36**, 9797 (1987).
[47] J. E. Reutt, Y. J. Chabal, and S. B. Christman, J. Electron Spectrosc. Relat. Phenom. **44**, 325 (1987).
[48] E. G. Seebauer and L. D. Schmidt, Chem. Phys. Lett. **123**, 129 (1986).
[49] A. P. Graham, A. Menzel, and J. P. Toennies, J. Chem. Phys. **111**, 1676 (1999).
[50] W. Eberhardt, F. Greuter, and E. W. Plummer, Phys. Rev. Lett. **46**, 1085 (1981).
[51] J. Lee, J. P. Cowin, and L. Wharton, Surf. Sci. **130**, 1 (1983).
[52] W. Di, K.E. Smith, and S. D. Kevan, Phys. Rev. B **45**, 3652 (1992).
[53] S Wehner and J. Küppers, J. Chem. Phys. **108**, 3353 (1998).
[54] S. Wehner and J. Küppers, Surf. Sci. **411**, 46 (1998).
[55] P. J. Feibelman and D. R. Hamann, Surf. Sci. **182**, 411 (1987).
[56] B. Hammer and J. K. Nørskov, Surf. Sci. **343**, 211 (1995).
[57] A. T. Pasteur, S. J. Dixon-Warren, Q. Ge, and D. A. King, J. Chem. Phys. **106**, 8896 (1997).
[58] R. J. Gale, M. Salmeron, and G. A. Somorjai, Phys. Rev. Lett. **38**, 1027 (1977).
[59] M. Salmeron, R. J. Gale, and G. A. Somorjai, J. Chem. Phys. **67**, 5324 (1977).
[60] E. Pijper, G. J. Kroes, R. A. Olsen, and E. J. Baerends (in preparation).